Entanglement transition through Hilbert-space localization

Quancheng Liu[1] and Klaus Ziegler [2,*]

[1]*Department of Physics, Institute of Nanotechnology and Advanced Materials, Bar-Ilan University, Ramat-Gan 52900, Israel*
[2]*Institut für Physik, Universität Augsburg, D-86135 Augsburg, Germany*

We study Hilbert-space localization of the many-body dynamics due to ergodicity breaking and analyze this effect in terms of the entanglement entropy and the entanglement spectrum. We find a transition from a regime driven by quantum tunneling to a regime that is dominated by boson-boson interaction, where the latter exhibits ergodicity breaking. Properties of this transition are captured by observation time averaging, which effectively suppresses the large dynamical entanglement fluctuations near the critical point. We employ this approach to the experimentally available bosonic Josephson junction. In this example, the transition from a tunneling regime to Hilbert-space localization reveals clear signatures in the entanglement entropy and entanglement spectrum. Interestingly, the transition point is reduced by quantum effects in comparison to the well-known result of the mean-field approximation in the form of self-trapping. This indicates that quantum fluctuations reduce the classical self-trapping. Different scaling with respect to the number of bosons, N, is found in the tunneling and the localization regime: While the entanglement entropy grows *logarithmically* with N in the tunneling regime, it increases *linearly* in the localized regime. Our results indicate that entanglement provides a concept for a sensitive diagnosis for the transition from a quantum tunneling regime to Hilbert-space localization.

I. INTRODUCTION

Entanglement is considered as one of the most fundamental building blocks in quantum physics and quantum information processing. Specifically, the Rényi entanglement entropy measures the quantum correlations between two subsystems under a spatial bipartition [1–4], which has become an important and popular concept for detecting measurement-induced entanglement transitions [5–7], characterizing many-body dynamics and localization [8–17], and classifying the topology of quantum systems [18–21]. Recently, the Rényi entanglement entropy has been efficiently measured in the laboratory with randomized methods without full quantum state tomography [22–24].

Hilbert-space localization (HSL) describes the phenomenon in which the evolution of a quantum system from an initial Fock state is restricted to a subregion of the Hilbert space in the presence of strong particle-particle interaction, i.e., it is a special form of spontaneous ergodicity breaking. It originates from the fact that a Fock state is an eigenstate of the local interaction part of the Hamiltonian, where only a sufficiently strong tunneling can overcome the HSL. Although we anticipate such a behavior for any system in which tunneling competes with particle-particle interaction, so far it was only calculated for the bosonic Josephson junction (BJJ). In this case, we have seen that it is characterized by a change of the scaling behavior of the participation ratio [25] or by a sudden jump of the return probability between different states [26]. The dynamics of the system is rather complex,

where the scattering of an individual particle by other particles can be considered as random. Therefore, HSL is reminiscent of Anderson localization in real space [27], with the crucial difference that the scattering environment in the latter is static rather than dynamic. It also distinguishes itself from other types of many-body localization, where the interplay of interactions and disorder is involved [8,9,28]. In this article, we focus on the BJJ, which has been studied intensively in the semiclassical limit [29–32] and realized experimentally [33–37]. It is found that the entanglement transition and different properties are strongly related to the HSL.

The implementation of entanglement in the investigation of many-body localization has led to some of the most important discoveries in many-body physics. For example, the scaling laws of Rényi entanglement entropy are taken as the key characteristic of the many-body localization phase. Nevertheless, it is still unclear how the entanglement behaves when a many-body system undergoes the HSL phase transition, arising from the competition of particle interactions and tunneling. Here we investigate the following questions: Is there a generic entanglement transition and HSL correspondence? Will the entanglement exhibit different characteristic properties in the localized and tunneling phases? Can entanglement reveal quantum effects that are not covered by the classical mean-field approximation? Affirmative answers are obtained in this work.

The unitary evolution of a quantum system typically drives it to states of higher entanglement [6,38] and the dynamical entanglement entropy usually exhibits large fluctuations, which makes it difficult to extract generic information about the system. Here we adopt the principle of ensemble average from statistical physics for the ensemble created by

*klaus.ziegler@physik.uni-augsburg.de

012413-1

randomly chosen observation times. We denote this approach as the observation time average method. In the experiment, this means one repeats the measurement at different times on identical systems and averages over this ensemble of results. This idea has some similarities with the random matrix theory, where averaging an ensemble of Hamiltonians is used to obtain generic properties of the many-body spectrum [39–44]. It is shown that the observation time average method is a powerful tool and efficiently suppresses the randomness in entanglement entropy and entanglement spectrum. Moreover, this approach can be extended to the investigation of other systems with entanglement.

II. MODEL

Within the single-mode approximation [29], the BJJ with N bosons can be described as a two-site Bose-Hubbard model,

$$H_{\text{BJJ}} = -J(a_L^\dagger a_R + a_R^\dagger a_L) + \frac{U}{2}(n_L^2 + n_R^2), \qquad (1)$$

where $a_{L,R}^\dagger$ ($a_{L,R}$) are the bosonic creation (annihilation) operators in the left and right potential traps, and $n_{L,R} = a_{L,R}^\dagger a_{L,R}$ are the corresponding number operators. J describes the tunneling of bosons between the traps and U represents the particle-particle interaction, which energetically favors a symmetric distribution of bosons in the double traps when $U > 0$. Using Fock states $|k, N-k\rangle \equiv |k\rangle \otimes |N-k\rangle$ ($k = 0, \ldots, N$) as a basis of the Hilbert space, the corresponding Hamiltonian matrix has a tridiagonal structure with $H_{k,k'} = \langle k, N-k|H_{\text{BJJ}}|k', N-k'\rangle = U[(N-k)^2 + k^2]\delta_{k,k'} - J\sqrt{k(N+1-k)}\delta_{k,k'-1} - J\sqrt{k'(N+1-k')}\delta_{k,k'+1}$. This matrix can be interpreted as a $(N+1)$-site tight-binding lattice with broken translational invariance, where the tunneling rate and the potential are minimal at the center and grow symmetrically towards the endpoints. Hence, the HSL in the BJJ is related to translation symmetry breaking, in contrast to Anderson localization in the presence of quenched disorder [27], whose ensemble is translational invariant. Using the SU(2) spin representation, the BJJ Hamiltonian can also be written as [29]

$$H_{\text{BJJ}}^S = UL_z^2 - 2JL_x + UN^2/4, \qquad (2)$$

when $L_x = (a_L^\dagger a_R + a_R^\dagger a_L)/2$ and $L_z = (a_L^\dagger a_L - a_R^\dagger a_R)/2$, representing a large nonlinear spin system with magnitude $S = N/2$. This maps the evolution of BJJ to the spin motion on the Bloch sphere.

III. ENTANGLEMENT AND RÉNYI ENTROPY

The Hilbert space $\mathcal{H}$ of the BJJ is a product space $\mathcal{H}_l \otimes \mathcal{H}_r$ that comprises the left and right traps. We start with all bosons in the right well, i.e., $\rho_0 = |0, N\rangle\langle0, N|$. On the Bloch sphere, the initial spin vector $\langle0, N|\mathbf{L}|0, N\rangle$ [$\mathbf{L} = (L_x, L_y, L_z)$] points to the south pole [Fig. 2(a)]. This is a high-energy state with $E = UN^2/2$ and the left and right traps are not entangled. With Eq. (1), the unitary evolution density operator reads $\rho(t) = e^{-iH_{\text{BJJ}}t}\rho_0 e^{iH_{\text{BJJ}}t}$. We define the reduced density matrix $\rho_L(t) = \text{Tr}_R[\rho(t)]$ with respect to the right well by summing over all possible states in the right well. This gives an $(N+1) \times (N+1)$ matrix with elements
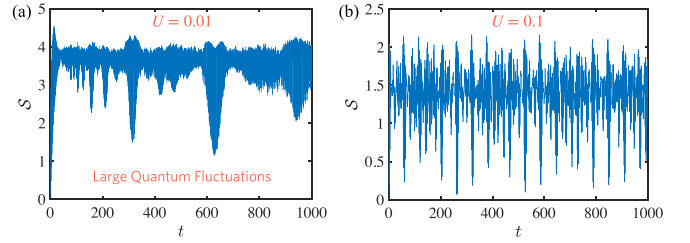

FIG. 1. The entanglement entropy $\mathcal{S}$ for 100 bosons as a function of time t for (a) $U = 0.01$ and (b) $U = 0.1$. We set $J = 1$. As shown in the figure, the entanglement entropy fluctuates strongly in time, which is later suppressed with the observation time average.

$\rho_{nn'}^L(t) = \sum_{k=0}^N \langle n, k|\rho(t)|n', k\rangle$. Only $k = N - n' = N - n$ survive in the summation due to particle number conservation. This implies a diagonal reduced density matrix,

$$\rho_L(t) = \text{Tr}_R \rho(t) = \begin{bmatrix} \rho_0^L(t) & & \\ & \ddots & \\ & & \rho_N^L(t) \end{bmatrix}, \qquad (3)$$

with elements $\rho_n^L(t) = \langle n, N-n|\rho(t)|n, N-n\rangle$. For $t = 0$, the $\rho(t)$ and $\rho_L(t)$ both have only a single nonzero matrix element, namely, $\rho_{0,N;0,N}(t=0) = \rho_0^L(t=0) = 1$. Localization is characterized by a large weight of only a few matrix elements for all $t > 0$, while for a delocalized state, the weight is distributed over time $t > 0$ to all states, such that $\rho_k^L(t) \approx 1/(N+1)$.

With $\rho_L(t)$, we introduce the Rényi entropy [16] as a quantitative measure for the entanglement between the traps, which gives

$$\mathcal{S}_\alpha(t) = \frac{1}{1-\alpha} \log_2 \text{Tr}[\rho_L^\alpha(t)] = \frac{1}{1-\alpha} \log_2 \sum_n [\rho_n^L(t)]^\alpha. \qquad (4)$$

In general, α is a free parameter and the typical values used are $\alpha = 2, 3$ [16]. We fix $\alpha = 2$ in the subsequent calculations. $\mathcal{S}(t) \equiv \mathcal{S}_2(t)$ measures the entanglement entropy over time with the initial value $\mathcal{S}(t=0) = 0$. With Eqs. (3) and (4), we plot the entanglement entropy versus time for $N = 100$ bosons with $J = 1$ and $U = 0.01$ or 0.1 separately in Fig. 1. The unitary evolution drives the system into higher entangled states rapidly, indicating the fast entanglement growth at the beginning. In the long-time limit, the mean entanglement entropy saturates but is subject to strong fluctuations. The mean value depends on the system parameters. For instance, with $U = 0.01$ ($U = 0.1$), we obtain $\mathcal{S} \sim 3.8$ ($\mathcal{S} \sim 1.5$).

IV. RANDOM OBSERVATION TIME

To reveal the generic entanglement dependence on the system parameters such as N, J, and U, we need to avoid large quantum fluctuations. This is done by the observation time average method: We conduct a specific experiment (or perform a calculation) repeatedly at different times and average with respect to those times. In other words, we perform a time average of the observables. This is applied to the reduced
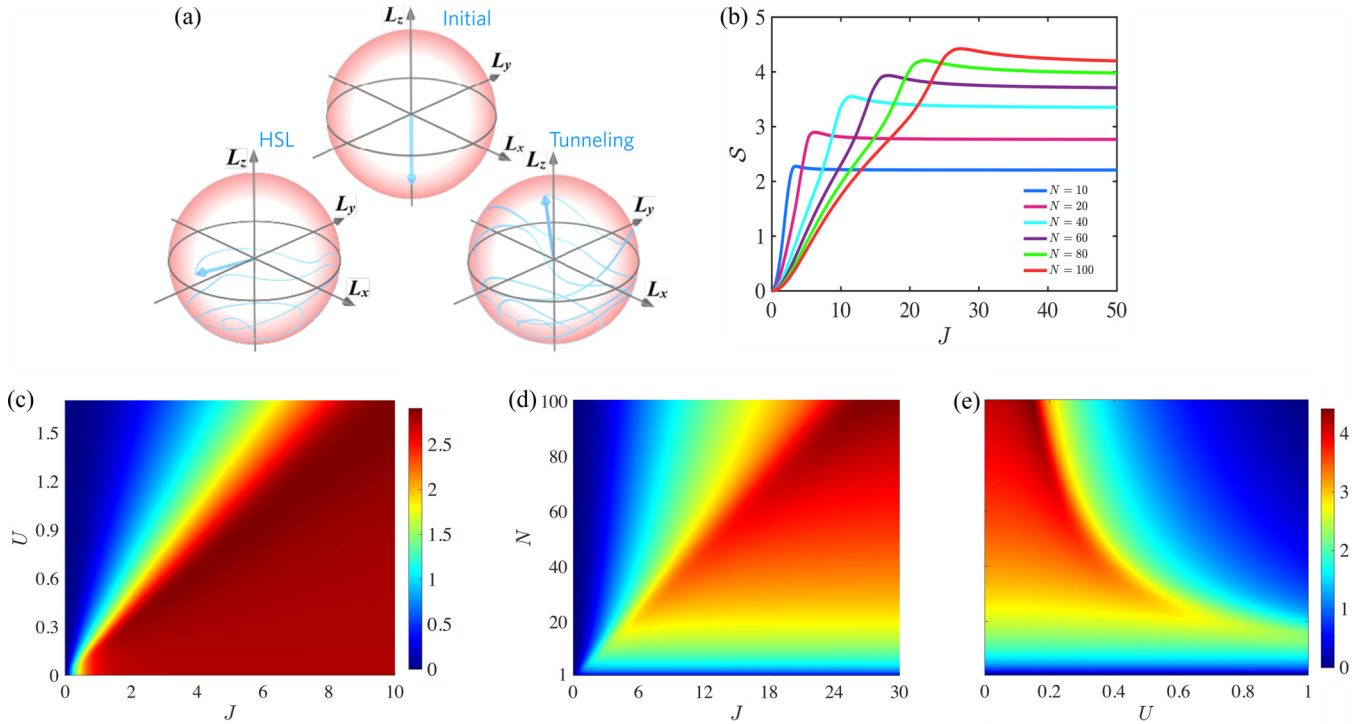
FIG. 2. The entanglement entropy phase transition with system parameters. (a) Schematic plot of the HSL phase and tunneling phase on the Bloch sphere. (b) Plot of $\mathcal{S}(J)$ for different Ns with $U = 1$. When J is small, corresponding to the HSL phase, $\mathcal{S}$ increases with J. The system undergoes the phase transition to the tunneling regime at J_c, after which $\mathcal{S}$ is a constant. (c) The competition of U and J, where we choose $N = 20$ and the colors represent the magnitude of $\mathcal{S}$. (d),(e) The effects of the number of bosons on the phase transition. Specifically, (d) $\mathcal{S}(J, N)$ with $U = 1$ and (e) $\mathcal{S}(U, N)$ with $J = 1$. The four plots (b)–(e) indicate a clear entanglement phase transition when the system undergoes the transition from the HSL phase to the tunneling phase controlled by the U, J, and N.

density matrix of the BJJ and gives

$$\left\langle \rho_n^L(t) \right\rangle_t = \sum_{j,j'=0}^{N} c_n(E_j, E_{j'}) \langle e^{-i(E_j - E_{j'})t} \rangle_t, \quad (5)$$

where the matrix element $c_n(E_j, E_{j'}) = \langle N - n, n | E_j \rangle \langle E_j | \rho_0 | E_{j'} \rangle \langle E_{j'} | N - n, n \rangle$, where $|E_j\rangle$ (E_j) is an eigenstate (eigenvalue) of the Hamiltonian H_{BJJ}. For the observation time average $\langle \cdot \rangle_t$, we choose the exponential distribution $se^{-st}dt$, where long-time observations are exponentially suppressed on the scale $1/s$. This gives $\langle e^{-i(E_j - E_{j'})t} \rangle_t = 1/[1 + i(E_j - E_{j'})/s]$, which indicates that the effective evolution after average is no longer unitary. The probability is preserved, though, since $\sum_n \langle \rho_n^L(t) \rangle_t = 1$, reflecting the absence of losses in the closed system. Therefore, the observation time average is different from random weak measurements. With Eq. (3), the observation time average gives, for the diagonal reduced density matrix $\langle \rho_L(t) \rangle_t$ with elements,

$$\left\langle \rho_n^L(t) \right\rangle_t = \int_0^\infty \rho_n^L(t) se^{-st} dt = \sum_{j,j'=0}^{N} \frac{c_n(E_j, E_{j'})}{1 + i(E_j - E_{j'})/s}, \quad (6)$$

where $s = 1$ is subsequently used. This expression is used to calculate the corresponding Rényi entanglement entropy $\mathcal{S}(J, U, N)$ with Eq. (4), where the entropy is a function of N, U, J without fluctuations in time. As shown in Fig. 2, the

time average leads to a smooth behavior of the entanglement entropy for the system parameters, where the entanglement transition by the HSL is clearly presented.

In Figs. 2(b) and 2(d), we plot $\mathcal{S}(J)$ for different numbers of bosons. Physically, when J is small, i.e., in the HSL phase, the motion of the bosons is constrained to the southern hemisphere [Fig. 2(a)] and the matrix element $\langle N - k, k | H_{\mathrm{BJJ}} | 0, N \rangle = -J \langle k, N - k | a_L^\dagger a_R + a_R^\dagger a_L | 0, N \rangle$ is very small and proportional to J (for fixed N). This is exactly reflected in the entanglement entropy, where $\mathcal{S}(J)$ grows approximately linearly with J until it reaches the critical value J_c [Fig. 2(b)]. The J_c is the transition point of the HSL phase to the tunneling phase, after which the bosons can reach the entire Hilbert space from the initial state [Fig. 2(a)]. This explains why, in the tunneling regime, the $\mathcal{S}(J)$ is a constant and only depends on the size of the system [Fig. 2(d)], meaning the entanglement entropy measures to what extent the system can explore the Hilbert space. In Fig. 2(c), the competition between the tunneling J and particle interactions U for $N = 20$ is presented. When increasing U, it takes a larger value of J to reach the entanglement phase transition. In the HSL phase, the $\mathcal{S}(J, U)$ is proportional to J and inversely proportional to U. While in the tunneling regime, $\mathcal{S}(J, U)$ is a constant, when the entire Hilbert space is accessible. In Fig. 2(e), we plot $\mathcal{S}(U, N)$, where the size effects on the entanglement phase transition are shown. When the number of bosons is large, the system is more easily localized in the
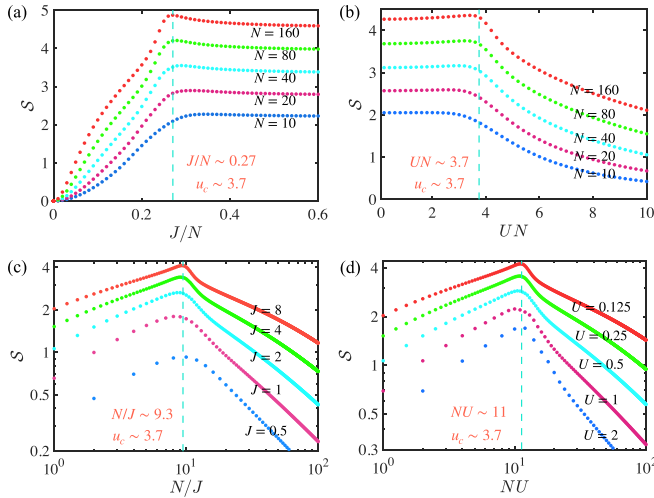
FIG. 3. The characterization of the critical transition point u_c. (a) Plot of $\mathcal{S}$ vs J rescaled by N with $U = 1$. (b) Similarly, $\mathcal{S}(UN)$ with $J = 1$. The phase transition point $u_c \sim 3.7$ for all the realizations. We plot the dependence of the entanglement entropy with N, (c) rescaled by J^{-1} with $U = 0.4$ and (d) rescaled by U with $J = 3$. Again, the entanglement entropy undergoes a phase transition at $u_c \sim 3.7$ and reaches the maximum at this critical value. Hence, u_c is a generic value that characterizes the entanglement phase transition.

Hilbert space and undergoes the entanglement phase transition for smaller values of U, since the critical value $u_c = UN/J$ does not depend on N. The critical entanglement phase transition point is shown in Fig. 3 with the characteristic parameter $u = UN/J$, which reveals a sharp boundary between the tunneling and HSL phases. In Fig. 3(a), we plot the $\mathcal{S}$ versus J rescaled by the N. Here, U is set to 1 and the entanglement entropy undergoes the phase transition, for different numbers of bosons, at the same value of $J/N \sim 0.27$. The critical point $u_c = UN/J \sim 3.7$. Similarly, we plot $\mathcal{S}(U, N)$ for different Ns in Fig. 3(b), where the system also exhibits the entanglement transition at $u_c \sim 3.7$. This generic phase transition behavior is also confirmed by tuning N with the rescaling by J^{-1} [Fig. 3(c)] and U [Fig. 3(d)], where the entanglement reaches its maximum at $u_c \sim 3.7$. Interestingly, this quantum phase transition point deviates from the results by the Gross-Pitaevskii equation [29] under the mean-field approximation, where

$$3.7 \approx u_c^{\text{Quantum}} < u_c^{\text{Mean field}} = 4. \tag{7}$$

It is crucial to note that both critical values depend on the number of bosons, N, only through the combination of parameters $u = UN/J$, as demonstrated in Fig. 3. This fact, as well as the critical value $u_c^{\text{Quantum}} \approx 3.7$, were also found previously for the scaling change of the participation ratio [25] and for the jump of the return probability [26]. The above result reflects the effective enhancement of the particle-particle interaction by quantum entanglement, where the system undergoes the HSL phase transition with smaller U's and causes quantitative change in the entropy. In contrast, the mean-field approximation ignores the entanglement and, therefore, it requires a stronger particle-particle interaction to reach the self-trapping transition. The deviation of u_c from its

mean-field value is in agreement with a recent work by Wimberger *et al.* on the N dependence of u_c for different initial states [32]. Their critical values are monotonically increasing even up to $N \approx 100$, in contrast to Fig. 3. This indicates that the observation time averaged entanglement entropy (EE) provides a more stable criterion for the definition of a critical point.

Our calculations are limited to $N \approx 100$ bosons. It would be interesting though to calculate the critical value u_c also in the large-N regime. The fact that the EE increases monotonically with N in Fig. 3 indicates that a classical description with only a one-particle mean-field wave function for the two sites of the BJJ might not be sufficient, at least for $u \approx u_c$. A semiclassical approximation has been used as an interpolation between the full quantum evolution and the classical approximation, where large values of N are accessible [30,32]. Such calculations reveal that the value of u_c varies for different initial states. Moreover, the fluctuations decay very slowly with N in the vicinity of u_c [30].

Different scaling behaviors with the size of the system are found in the HSL phase and tunneling phase. Here we use the normalized entanglement entropy defined by $\widetilde{\mathcal{S}} = \mathcal{S}/\mathcal{S}_{\max}$ for constant u. As shown in Figs. 4(a) and 4(c), we plot $\widetilde{\mathcal{S}}$ versus the number of bosons, N, keeping characteristic parameter u a constant [$u = 1 < u_c$ for Fig. 4(a) and $u = 40 > u_c$ for Fig. 4(c)]. Note that as $u \sim J^{-1}$ and $u \sim UN$, the small u corresponds to the tunneling phase and large u corresponds to the HSL phase. The entanglement entropy increases logarithmically with the size of the system for the tunneling regime and linearly for the localized regime, namely,

$$\widetilde{\mathcal{S}} \sim \ln(N),\ u < u_c; \quad \widetilde{\mathcal{S}} \sim N,\ u > u_c. \tag{8}$$

The linear N behavior is counterintuitive when we follow the argument of a single localized state. In the present model, though, localization appears in a two-dimensional space that includes two Fock states. This is a consequence of the mirror symmetry of the BJJ model. Then the EE reads $\widetilde{\mathcal{S}} \sim -\log_2[\rho_N^2 + (1 - \rho_N)^2] \sim 2\rho_N$ with $\rho_N \sim cN$. This was confirmed in a direct calculation of the reduced density matrix with $c \approx 0.002$ (cf. Appendix). Then the linear N behavior is valid in a crossover region up to $N \approx 200$, but becomes asymptotically $\rho_N \sim 1/2$. The transition of scaling behaviors around $u_c \sim 3.7$ is clearly visualized in Fig. 4(b). The linear increase reflects the fact that a fixed fraction of states is localized, and the entanglement entropy increases with the effective volume of the traced right well. This is obviously quite different from the tunneling regime, where the entire Hilbert space is involved, implying that the matrix elements of the reduced density matrix are equally distributed, leading to a $\ln N$ behavior. This logarithmic behavior can be considered a modification of the area law, which is initially proposed for noninteracting particles.

Quite generally, a degeneracy in the energy spectrum can be associated with a phase transition. For instance, a typical quantum phase transition is associated with the degeneracy of the ground state. Then an important question is whether the above entanglement phase transition reveals some characteristic features in the entanglement spectrum [45], which is defined as the eigenvalues of the reduced density matrix. The concept of entanglement spectrum is utilized in the detecting
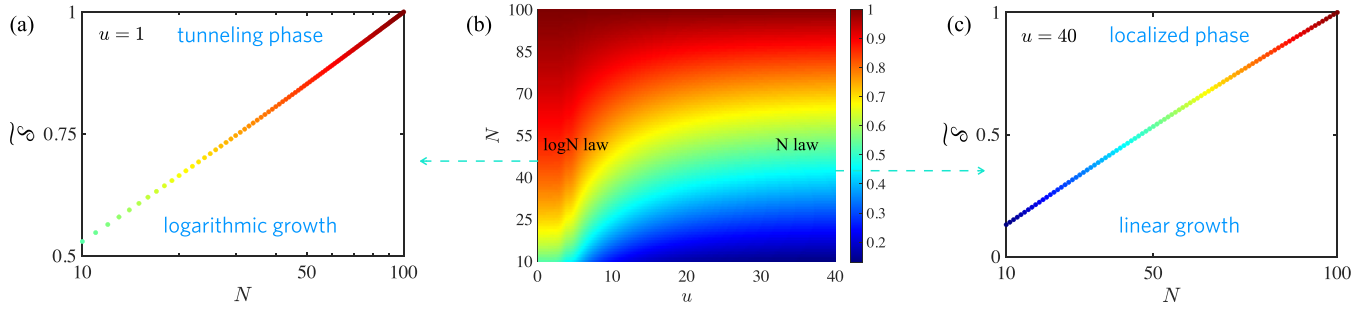
FIG. 4. Scaling laws for the tunneling and HSL phases. (a) Plot of normalized entanglement entropy vs the number of bosons, N, with $u = 1$. Here, $u < u_c \sim 3.7$, corresponding to the tunneling phase; $\widetilde{S}$ grows logarithmically with N. (c) Different scaling behaviors are found when the system is in the HSL phase, where $\widetilde{S}$ increases linearly with N. (b) Plot of $\widetilde{S}(u, N)$ with color representing its magnitude. The scaling law keeps $\widetilde{S} \sim \ln N$ when $u < u_c$ and gradually becomes $\widetilde{S} \sim N$ after crossing the transition point u_c.

of topological orders [46] and extensively investigated with different lattice models [47,48]. In the case of the evolution with excited states, the relation between the phase transition and the entanglement spectrum can be very complex because, as in the case of HSL, it is not a transition associated with the ground state alone. Here, the diagonal form of the reduced density matrix in Eq. (3) enables the direct calculation of the entanglement spectrum. Together with Eq. (6), we have

$$\xi_n = \ln \left[\langle \rho_n^L(t) \rangle_t \right]. \tag{9}$$

Here we use the time-independent reduced matrix to avoid the fluctuations, as we have discussed. We plot the entanglement spectrum $\xi_n(U)$ in Fig. 5(a) and $\xi_n(J)$ in Fig. 5(b) for $N = 10$, where the entanglement transition clearly exhibits signatures in the spectrum. Specifically, the entanglement spectrum has almost constant levels independent of U and J in the tunneling phase and repulsive levels in the HSL phase. The transition from constant levels to repulsive levels happens exactly at the critical transition point u_c, as we find for the entanglement entropy. Thus, the entanglement spectrum is also a useful indicator for observing a qualitative change in the onset of the HSL transition. In particular, the strong level repulsion in the localized regime with increasing U is significant.

V. SUMMARY AND DISCUSSION

We have investigated the entanglement phase transition that arises from the competition between the tunneling and particle-particle interaction, where both entanglement entropy

and entanglement spectrum undergo a clear quantum phase transition from the tunneling regime to the HSL regime. It is crucial though to apply the observation time average to suppress strong quantum fluctuations in time, which is a powerful tool and can be extended for other studies on entanglement. Moreover, the transition point we find here is smaller than the value given by the mean-field approximation with the Gross-Pitaevskii equation. This reveals the quantum effects that are not covered in the form of self-trapping. Different scaling laws with the size of the system are found before and after the phase transition. It is shown that the entanglement entropy grows logarithmically with the number of bosons in the tunneling phase and linearly in the localized phase.

Our results indicate that the entanglement entropy (entanglement spectrum) can be controlled by the tunneling rate J, interaction strength U, and the number of the bosons, N, which can be proven in the present experiment platforms. For instance, for an ultracold Bose gas in a two-site optical lattice, the potential barrier can be tuned by an external laser field [36]. Another realization of a BJJ is a pair of coupled polariton condensates [34]. In such experiments, by tuning the parameters in the setup, critical phase transitions may be observed. The generalization of the two-site structure of the BJJ to more sites should provide similar effects of controllable entanglement and HSL, reflecting that the two-site prototype is a scalable model. Another extension of the BJJ is the coupling to a large but finite bath [49]. Then we expect similar localization and entanglement effects as we found here.

FIG. 5. Entanglement spectrum as a function of (a) U and (b) J. The transition to the HSL is indicated by the repulsion of the levels, which keeps constant in the tunneling phase and spreads in the HSL phase. Compared with the entanglement entropy, the critical transition of the entanglement spectrum is again characterized by u_c.

APPENDIX: EVOLUTION OF THE ENTANGLEMENT ENTROPY

The EE is given by the reduced density matrix $\hat{\rho}$ through the Rényi entropy. Thus, the evolution of the EE is determined by the evolution of $\hat{\rho}$, whose diagonal elements can be written
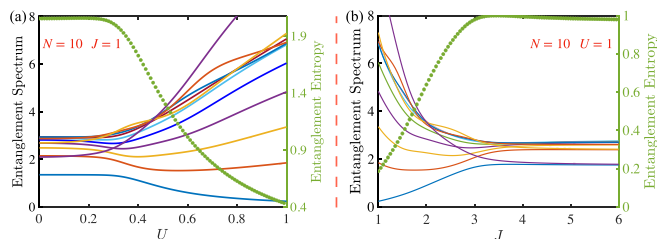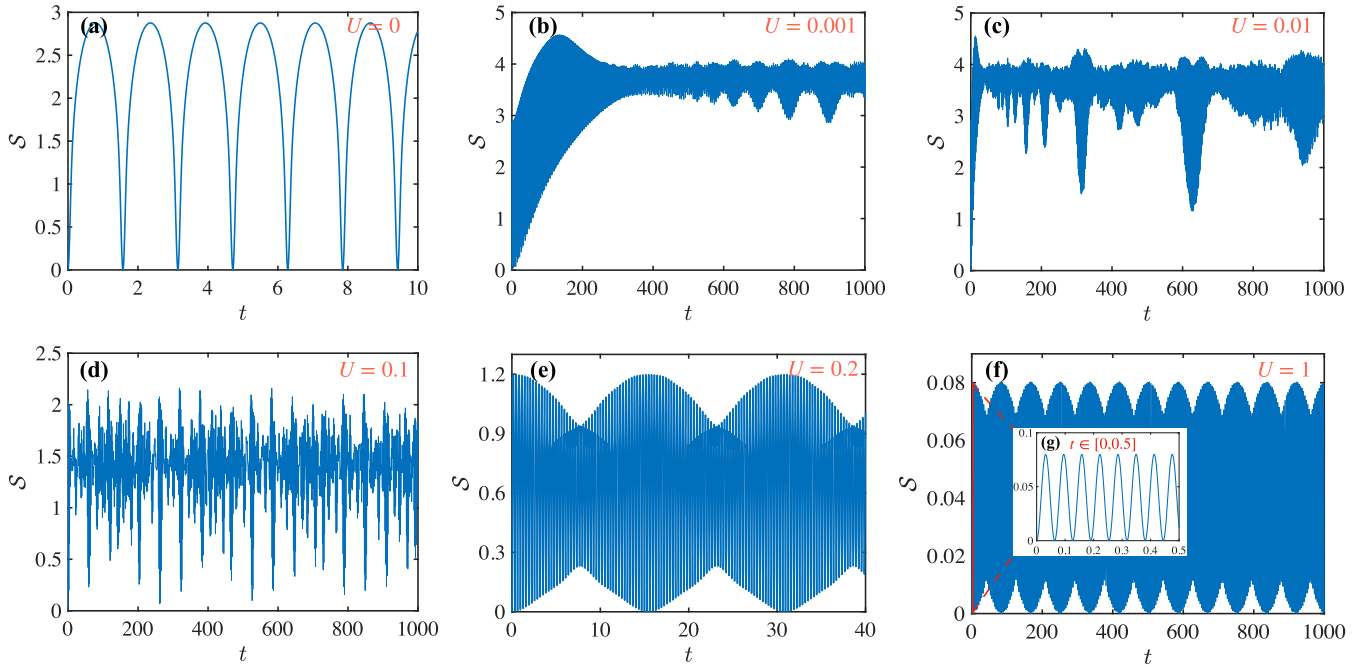
FIG. 6. Evolution of the EE for $N = 100$ bosons with $J = 1$ and different values of the interaction strength U on different timescales.

in spectral representation as

$$\hat{\rho}_n(t) = \langle n, N - n | e^{-iHt} | 0, N \rangle \langle 0, N | e^{iHt} | n, N - n \rangle$$

$$= \sum_{j,j'=0}^{N} e^{-i(E_j - E_{j'})t}$$

$$\times \langle n, N - n | E_j \rangle \langle E_j | 0, N \rangle \langle 0, N | E_{j'} \rangle \langle E_{j'} | n, N - n \rangle.$$
$$(A1)$$

This is a superposition of oscillating functions with frequencies $\{|E_j - E_{j'}|\}$, where the fastest oscillations are given by the largest frequency. We can distinguish two extreme cases for the BJJ: the noninteracting case with $U = 0$ and the nontunneling case with $J = 0$. For $U = 0$, the energy spectrum is equidistant with distance $2J$ and energy eigenvalues $E_0 = 0$, $E_j = \pm 2Jj$ ($j = 1, 2, \ldots, N/2$) [50]. This implies a periodic evolution with period $t_p = \pi/2J$. In particular, the matrix elements of the density matrix elements with $n = 0, N$ read $\hat{\rho}_0(t) = |\cos(Jt)|^{2N}$ and $\hat{\rho}_N(t) = |\sin(Jt)|^{2N}$ [51]. This is reflected by the behavior visualized in Fig. 6(a). The other extreme is $J = 0$. Since the initial state $|0, N\rangle$ is an eigenstate of the Hamiltonian, there is no evolution. A small tunneling rate J, though, splits the degeneracy of $|0, N\rangle$ and $|N, 0\rangle$ and creates a small frequency of the order of J that leads to very slow oscillations in the evolution. On the other hand, the fastest oscillations are caused by the maximal frequency $UN^2/4$. This is visible in Fig. 6(f).

The evolution is more complex in the intermediate regime, where tunneling and interaction compete. Different frequencies contribute and there is an evolution on all timescales, caused by frequencies from 0 to the largest frequency $UN^2/4$. The oscillating behavior is only limited by the number of frequencies, $N_f = (N + 1)N/2$. Typical examples of the EE in the BJJ are plotted in Fig. 6 on different timescales. The

influence of the interaction strength U clearly distinguishes a noninteracting tunneling regime [Fig. 6(a)] and a strongly interacting regime of fast oscillations with $t_p \approx 0.07$ [inset in Fig. 6(f)] and slower oscillations with $t'_p \approx 90$, where the EE is quite small. There is an intermediate regime that has characteristic features on long timescales that represents small frequencies. Moreover, the intermediate regime has a higher EE than the other two regimes. This indicates a more complex evolution. In Fig. 7, the evolution of the EE is compared on the same timescale for the different regimes.

Besides the frequencies of the oscillations, the expansion coefficients in (A1) play a crucial role in the evolution. They reflect the overlap between the Fock states and the energy eigenstates and determine the entanglement of the different Fock states. In the tunneling regime, all elements of the reduced density matrix contribute significantly, for instance, at time $t = 1000$ [cf. Fig. 8(a)]. In the localized regime, on the other hand, the overlaps between the Fock states with a few energy eigenstates are large. In particular, for $J = 0$, we get $\hat{\rho}_n(t) = \delta_{nN}$, which yields a vanishing EE. Small tunneling
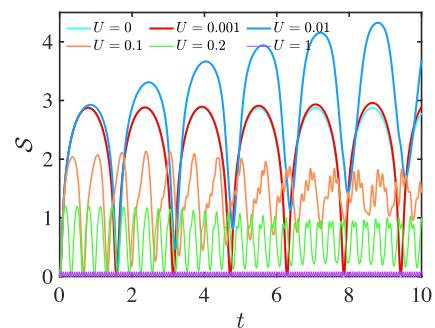

FIG. 7. Evolution of the EE for different values of U, $J = 1$, and $N = 100$ on the same timescale.
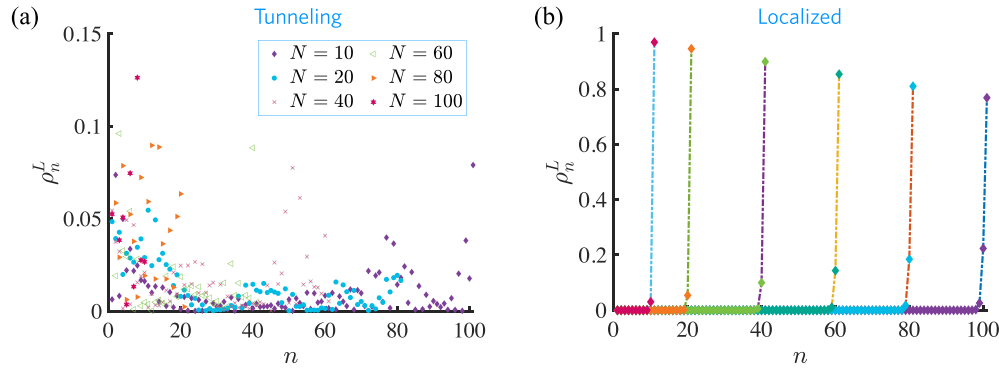
FIG. 8. The elements $\rho_n^L(t)$ of the reduced density matrix for different numbers of bosons N (a) Deep in the tunneling regime ($u = 1$) at fixed time $t = 1000$ and (b) deep in the localized regime ($u = 40$), where the maximum of $\rho_n^L(t)$ on the time interval $[0, 2000]$ is plotted.

can be treated as a perturbation expansion in powers of J, leading to a small EE. In this case, the elements of the reduced density matrix have only two significant contributions, as visualized in Fig. 8(b). A special effect is that for a fixed u, the smaller of the two matrix elements increases linearly with N such as $2N/1000$ up to $N \approx 200$ bosons. We anticipate a saturation for larger values of N, which eventually results in two equal matrix elements of $1/2$.

These time-dependent results indicate a complex evolution of the reduced density matrix and the EE that is caused by the oscillating behavior with various frequencies. Degeneracies in the energy spectrum due to specific physical effects, such as phase transitions, appear on large timescales. This fact suggests that the oscillating behavior of the reduced density matrix on short timescales should be averaged out.

[1] L. Bombelli, R. K. Koul, J. Lee, and R. D. Sorkin, Phys. Rev. D **34**, 373 (1986).

[2] M. Srednicki, Phys. Rev. Lett. **71**, 666 (1993).

[3] J. Eisert, M. Cramer, and M. B. Plenio, Rev. Mod. Phys. **82**, 277 (2010).

[4] Q. Miao and T. Barthel, Phys. Rev. Lett. **127**, 040603 (2021).

[5] Y. Li, X. Chen, and M. P. A. Fisher, Phys. Rev. B **100**, 134306 (2019).

[6] B. Skinner, J. Ruhman, and A. Nahum, Phys. Rev. X **9**, 031009 (2019).

[7] O. Lunt, M. Szyniszewski, and A. Pal, Phys. Rev. B **104**, 155111 (2021).

[8] L. Amico, R. Fazio, A. Osterloh, and V. Vedral, Rev. Mod. Phys. **80**, 517 (2008).

[9] D. A. Abanin, E. Altman, I. Bloch, and M. Serbyn, Rev. Mod. Phys. **91**, 021001 (2019).

[10] G. Vidal, J. I. Latorre, E. Rico, and A. Kitaev, Phys. Rev. Lett. **90**, 227902 (2003).

[11] P. Calabrese and J. Cardy, J. Stat. Phys. Mech. (2004) P06002.

[12] I. Peschel and V. Eisler, J. Phys. A: Math. Theor. **42**, 504003 (2009).

[13] P. Calabrese and J. Cardy, J. Phys. A: Math. Theor. **42**, 504005 (2009).

[14] M. Serbyn, Z. Papić, and D. A. Abanin, Phys. Rev. X **5**, 041047 (2015).

[15] P. Kos, M. Ljubotina, and T. Prosen, Phys. Rev. X **8**, 021062 (2018).

[16] A. Chan, A. De Luca, and J. T. Chalker, Phys. Rev. X **8**, 041019 (2018).

[17] R. Nandkishore and D. A. Huse, Annu. Rev. Condens. Matter Phys. **6**, 15 (2015).

[18] M. Levin and X.-G. Wen, Phys. Rev. Lett. **96**, 110405 (2006).

[19] H. Yao and X.-L. Qi, Phys. Rev. Lett. **105**, 080501 (2010).

[20] H.-C. Jiang, Z. Wang, and L. Balents, Nat. Phys. **8**, 902 (2012).

[21] Q. Miao and T. Barthel, Quantum **6**, 642 (2022).

[22] S. J. van Enk and C. W. J. Beenakker, Phys. Rev. Lett. **108**, 110503 (2012).

[23] A. Elben, B. Vermersch, M. Dalmonte, J. I. Cirac, and P. Zoller, Phys. Rev. Lett. **120**, 050406 (2018).

[24] K. J. Satzinger *et al.*, Science **374**, 1237 (2021).

[25] D. Cohen, V. I. Yukalov, and K. Ziegler, Phys. Rev. A **93**, 042101 (2016).

[26] K. Ziegler, Symmetry **13**, 1796 (2021).

[27] P. W. Anderson, Phys. Rev. **109**, 1492 (1958).

[28] D. A. Huse, R. Nandkishore, V. Oganesyan, A. Pal, and S. L. Sondhi, Phys. Rev. B **88**, 014206 (2013).

[29] G. J. Milburn, J. Corney, E. M. Wright, and D. F. Walls, Phys. Rev. A **55**, 4318 (1997).

[30] M. Chuchem, K. Smith-Mannschott, M. Hiller, T. Kottos, A. Vardi, and D. Cohen, Phys. Rev. A **82**, 053617 (2010).

[31] S. Sinha and S. Sinha, Phys. Rev. Lett. **125**, 134101 (2020).

[32] S. Wimberger, G. Manganelli, A. Brollo, and L. Salasnich, Phys. Rev. A **103**, 023326 (2021).

[33] N. Bar-Gill, G. Kurizki, M. Oberthaler, and N. Davidson, Phys. Rev. A **80**, 053613 (2009).

[34] M. Abbarchi, A. Amo, V. G. Sala, D. D. Solnyshkov, H. Flayac, L. Ferrier, I. Sagnes, E. Galopin, A. Lemaître, G. Malpuech, and J. Bloch, Nat. Phys. **9**, 275 (2013).

[35] G. Spagnolli, G. Semeghini, L. Masi, G. Ferioli, A. Trenkwalder, S. Coop, M. Landini, L. Pezzè, G. Modugno, M. Inguscio, A. Smerzi, and M. Fattori, Phys. Rev. Lett. **118**, 230403 (2017).

[36] M. Pigneur, T. Berrada, M. Bonneau, T. Schumm, E. Demler, and J. Schmiedmayer, Phys. Rev. Lett. **120**, 173601 (2018).

[37] J.-F. Mennemann, I. E. Mazets, M. Pigneur, H. P. Stimming, N. J. Mauser, J. Schmiedmayer, and S. Erne, Phys. Rev. Res. **3**, 023197 (2021).

[38] H. Kim and D. A. Huse, Phys. Rev. Lett. **111**, 127205 (2013).

[39] E. P. Wigner, Ann. Math. **62**, 548 (1955).

[40] C. E. Porter and R. G. Thomas, Phys. Rev. **104**, 483 (1956).

[41] F. J. Dyson, J. Math. Phys. **3**, 140 (1962).

[42] E. P. Wigner, SIAM Rev. **9**, 1 (1967).

[43] M. L. Mehta, *Random Matrices* (Elsevier, New York, 2004).

[44] C. W. J. Beenakker, Rev. Mod. Phys. **69**, 731 (1997).

[45] H. Li and F. D. M. Haldane, Phys. Rev. Lett. **101**, 010504 (2008).

[46] Z. Gong and M. Ueda, Phys. Rev. Lett. **121**, 250601 (2018).

[47] F. Parisen Toldin and F. F. Assaad, Phys. Rev. Lett. **121**, 200602 (2018).

[48] P. Fries and I. A. Reyes, Phys. Rev. Lett. **123**, 211603 (2019).

[49] A. Riera-Campeny, A. Sanpera, and P. Strasberg, PRX Quantum **2**, 010340 (2021).

[50] K. Ziegler, Laser Phys. **22**, 331 (2012).

[51] K. Ziegler, Intl. J. Mod. Phys. B **31**, 1750255 (2017).